This is a preprint of an article accepted for publication in Journal of Seismology on 29 March 2013. The published article is available online at http://link.springer.com/article/10.1007/s10950-013-9358-3
To be cited as: Bouaanani N., Frasson-Botton C. 2013. Correlations of three-component ground motions from the 23 June 2010 Val-des-Bois, Québec, earthquake. Journal of Seismology, 17: 861–881.

Correlations of three-component ground motions from the 23 June 2010 Val-des-Bois, Québec, earthquake

Najib Bouaanani [1] and Cyril Frasson-Botton [2]

Abstract: In this paper, we investigate the characteristics of three-component ground motions recorded during the $M_{\mathrm{w}}\,5.2$ Val-des-Bois (Québec) earthquake, which occurred on the 23th June 2010. The earthquake is the largest recorded event in eastern Canada within the last decade. The records analyzed were provided by a strong motion monitoring network, comprising accelerometers located at sites with different soil conditions. The two orthogonal horizontal components and one vertical component at each recording station are uncorrelated to determine their principal directions, and the results obtained are used to characterize intensity ratios between the three uncorrelated components. A new hodograph representation is proposed to highlight the correlation between accelerations and displacement trajectories along various time increments at each recording station. The principal components are discussed in light of seismographic data, local site conditions and trajectories. Time-frequency analyses of the uncorrelated records are also conducted to compare the distribution of spectral amplitudes and frequency content along the three principal components during the shaking. The results of this work shed more light on the characteristics of three-component ground motions from an important ENA earthquake, and could be used to calibrate simulated multi-component ground motions in this region.

Key words: Eastern North America Seismicity; 3D ground motions; Earthquake principal components; Time-frequency analyses; Trajectories; Intensity ratios.

[1] Professor, Department of Civil, Geological and Mining Engineering,
Polytechnique Montréal, Montréal, QC H3C 3A7, Canada
Corresponding author. E-mail: najib.bouaanani@polymtl.ca
[2] Graduate Research Assistant, Department of Civil, Geological and Mining Engineering,
Polytechnique Montréal, Montréal, QC H3C 3A7, Canada.

1 Introduction

Eastern North America (ENA) experienced and will probably experience moderate-to-large intra-plate earthquakes that may pose significant hazard to population and infrastructure (Michel et al. 1990; Bruneau and Lamontagne 1994; Adams et al. 1995; Lamontagne et al. 2008). Research related to ENA particular seismotectonics and their effects has been hindered by the scarcity of recorded seismographic data. The $M_{\mathrm{w}}\,5.2$ Val-des-Bois (Québec) earthquake, which occurred on the 23th June 2010 and caused a significant shaking of the Ottawa urban area (Atkinson and Assatourians 2010; Lin et al. 2010), is the largest recorded event in eastern Canada within the last decade. The epicenter of the earthquake was located in Buckingham, within the Western Québec Seismic Zone (WQSZ), at latitude of $45.904\,^{\circ}$ N and longitude of $75.497\,^{\circ}$ W, approximately 60 km north of Ottawa (Ma and Motazedian 2012). The event was characterized as a northwest-striking thrust at a focal depth of about 22 km and was felt within large distances from the epicenter, far beyond Québec and Ontario, to reach Maine, Illinois and Kentucky (Atkinson and Assatourians 2010; Lin et al. 2010). The earthquake caused only limited damage near the epicentral region including cracked and fallen masonry elements, broken windows, a bridge embankment failure south of Bowman, Québec, and landslides triggered by the earthquake (Atkinson and Assatourians 2010; Geological Survey of Canada 2011).

The historical seismicity of the area includes $M\,5.8$ event of 1732 (near Montreal), $M\,6.2$ event of 1935 (Timiskaming) and $M\,5.6$ event of 1944 (Cornwall-Massena) (Lamontagne et al. 2008; Geological Survey of Canada 2011). The Val-des-Bois earthquake provided one of the richest recorded data sets in eastern Canada thanks to a recently installed strong motion monitoring network, comprising accelerometers located at sites with different soil conditions. In addition to the importance of such seismographic data in improving ENA ground motion prediction models, it also provides an important insight into the specificities of regional ENA seismic hazard, namely regarding the multi-component nature of the recorded ground motions through assessment of the corresponding three-component accelerations and displacements at the different recording sites. The characterization of multi-component ENA ground motions is indeed a first crucial step to ensure the appropriate selection of three-component seismic input for multidirectional 3D time-history or modal structural analyses. Such advanced analyses are now commonly used by structural engineers, because of the increasing geometrical complexity of structural systems, the greater expectations for analysis accuracy, and the availability of modern high performance computational tools. Several researchers such as López et al. (2006) have shown that the Arias intensities of the three-components of an earthquake are generally different, and that uncorrelated inter-component intensity ratios depend on regional seismic environments. Although significant research has been dedicated to studying ENA ground motions and their prediction, there is no published work investigating their uncorrelated components, defined in terms of two horizontal and one vertical accelerograms, as required by seismic safety evaluation of some critical structures. This paper aims at characterizing the correlations of three-component ground motions recorded during the $M_{\mathrm{w}}\,5.2$ Val-des-Bois earthquake. The records are processed to obtain uncorrelated principal components, and the uncorrelated ground motions are investigated in time and frequency

domains to characterize their relative amplitudes, intensities and frequency content.

2 Seismic data

In this paper, we study instrument-corrected ground motions recorded at stations located in Ottawa at epicentral distances ranging from 45 km to 65 km (Lin et al. 2010 ; Atkinson and Assatourians 2010). Figure 1 illustrates the epicenter and focal mechanism of the earthquake as well as the locations of the recording stations. Table 1 contains the station codes and coordinates (Lin et al. 2010), epicentral distances D_{E} and azimuths θ_{A} (Lin et al. 2010). The instrument sites, soil conditions and equivalent site classes (Adams 2007 ; Hunter et al. 2009) are also given in Table 1. The records at stations OTT, OTGH, OTNM and OTRS were provided by ETNA strong motion instruments, while those at stations OT002, OT004, OT006, OT008 and OT012 were obtained using Internet-Accelerometer (IA) instruments. The ETNA and IA instruments are operated by the Geological Survey of Canada and were installed between 2002 and 2005 at various sites of the Ottawa urban area to cover a wide range of typical soil conditions, varying from bedrock to thick layers of clay. The ETNA strong-motion instruments have limited on-site memory and operate in triggered mode with thresholds set appropriately to take each site's noise characteristics into account (Al-Khoubbi and Adams 2004 ; Adams 2007). They recorded the event at a rate of 200 samples per second, corresponding to accelerogram time steps of 0.005 s (Lin et al. 2010). The IA strong-motion instruments record data in continuous rather than triggered mode, and are permanently connected to the internet (Rosenberger et al. 2004 ; Adams 2007). They recorded the event at a rate of 100 samples per second, corresponding to accelerogram time steps of 0.01 s (Lin et al. 2010). The horizontal axes of all ETNA and IA instruments are oriented North-South and East-West. The peak ground accelerations (PGAs) of the two orthogonal horizontal components X (North-South), Y (East-West), and the vertical component Z of the records studied are given in Table 1. Figure 2 illustrates acceleration ratios a_i/a_{max}, $i = X, Y, Z$, where a_i is the recorded acceleration component and a_{max} the maximum of the three PGAs measured along each direction for a given site. For purpose of comparison, all the accelerograms are plotted over a same time interval of 100 s.

3 Correlation analyses of the recorded three-component ground motions

3.1 Review of the methodology used

The correlations between the three ground motion components recorded at each station are first investigated to assess the individual contributions of each component to the total energy released during the shaking. For this purpose, the methodology proposed by Penzien and Watabe (1975) is applied. We first determine the covariance matrix $\boldsymbol{\mu}$ of three translational time history accelerations $a_i(t)$, $i = X, Y, Z$, at a given site as

$$\boldsymbol{\mu} = \begin{bmatrix} \mu_{11} & \mu_{12} & \mu_{13} \\ \mu_{21} & \mu_{22} & \mu_{23} \\ \mu_{31} & \mu_{32} & \mu_{33} \end{bmatrix} \tag{1}$$

where the covariances are given by

$$\mu_{ij} = \frac{1}{t_\mathrm{f} - t_0} \int_{t_0}^{t_\mathrm{f}} a_i(t)\, a_j(t)\, \mathrm{d}t \qquad\qquad i,j = X,Y,Z \tag{2}$$

in which t_0 and t_f denote the first and last times of the interval of interest of the shaking duration, respectively. Applying a technique similar to finding the principal axes of a stress tensor (Popov 1990), a coordinate system in which matrix $\boldsymbol{\mu}$ is diagonal can be determined. These principal axes define directions along which earthquake signals are statistically uncorrelated. Denoting $\boldsymbol{\mu}_\mathrm{P}$ and $\boldsymbol{\alpha}_\mathrm{P}$ the principal covariances and orthogonal transformation matrices corresponding to this system, respectively, we have

$$\boldsymbol{\mu}_\mathrm{P} = \boldsymbol{\alpha}_\mathrm{P}^\mathrm{T}\, \boldsymbol{\mu}\, \boldsymbol{\alpha}_\mathrm{P} = \begin{bmatrix} \mu_1 & 0 & 0 \\ 0 & \mu_2 & 0 \\ 0 & 0 & \mu_3 \end{bmatrix} \tag{3}$$

The resulting principal variances μ_1, μ_2 and μ_3 are ordered as major, intermediate and minor, respectively: $\mu_1 \geqslant \mu_2 \geqslant \mu_3$. We mention that the covariances in Eq. (2) can be related to the tensor I of earthquake intensities defined by Arias (1970) as

$$I_{ij} = \frac{\pi}{2\mathrm{g}} \int_{t_0}^{t_\mathrm{f}} a_i(t)\, a_j(t)\, \mathrm{d}t \qquad i,j = X,Y,Z \tag{4}$$

where g is the acceleration due to gravity. This analogy allows a physical interpretation of the results by linking the principal axes to maximum, intermediate and minor directions along which maximum, intermediate and minor earthquake energy is released, respectively.

The time-dependency of the principal directions can be investigated by carrying out matrix transformations over small successive time intervals using a moving window technique (Båth 1974; Kubo and Penzien 1976). In this case, the time-dependent covariances μ_{ij} can be expressed as

$$\mu_{ij}(\bar{t}, \Delta t) = \frac{1}{\Delta t} \int_{\bar{t}-\frac{\Delta t}{2}}^{\bar{t}+\frac{\Delta t}{2}} a_i(t)\, a_j(t)\, \mathrm{d}t \qquad\qquad i,j = X,Y,Z \tag{5}$$

where $\bar{t}$ and Δt are the center and length of the moving time window, respectively. The time window length Δt has to be small enough to preserve signal nonstationarity, and large enough so that the time averaging in Eq. (5) remains valid.

3.2 Principal axes and intensity ratios

The eigenvectors corresponding to the principal variances are identified to distinguish the *most* vertical of the three principal axes, i.e. the eigenvector making the smallest angle with the geographical vertical axis Z at a given site (Penzien and Watabe 1975). This axis is denoted by V and the corresponding principal variance μ_V. The two other horizontal principal variances are denoted μ_{H_1} and μ_{H_2}, and are referred to as major and minor horizontal variances, respectively, with $\mu_{H_1} \geqslant \mu_{H_2}$. The corresponding eigenvectors identify the major and minor horizontal principal axes, respectively. The orientation of the principal axes can be defined using two principal angles θ_H and θ_V as illustrated in Figure 3:

– the horizontal principal angle θ_H between the projection $1'$ of the major horizontal principal axis and the epicentral direction relating the site to the epicenter. This angle varies between 0° and 180°, and is positive clockwise. Its value is 0° when the principal axis points to the epicenter.
– the vertical principal angle θ_V between the geographical vertical axis Z at the site and the *most* vertical principal axis V. This angle may vary between 0° and 90°, taking a value of 0° when axes V and Z coincide.

We also introduce the following variance or intensity ratios to characterize the relative importance of the uncorrelated components

$$\gamma_H = \frac{\mu_{H_2}}{\mu_{H_1}}\,; \qquad\qquad \gamma_V = \frac{\mu_V}{\mu_{H_1}} \tag{6}$$

We note that the ordering of the calculated vertical and horizontal principal variances cannot be predicted *a priori*. Any of the three following cases could then be expected

$$\mu_{H_1} \geqslant \mu_{H_2} \geqslant \mu_V\,; \qquad \mu_{H_1} \geqslant \mu_V \geqslant \mu_{H_2}\,; \qquad \mu_V \geqslant \mu_{H_1} \geqslant \mu_{H_2} \tag{7}$$

The order of the principal variances for a given ground motion is important since it informs on the relative significance of the three principal directions in terms of Arias intensity. It is particularly interesting to identify whether the vertical principal direction corresponds to the minor, intermediate or major variance. It is also useful to interpret the horizontal variance ratio γ_H as a measure of the relative importance of the intensities of the two horizontal principal components, and the vertical variance ratio γ_V as an indication of the relative importance of the intensity along the vertical direction.

3.3 Time-frequency analyses

The frequency content of a ground motion is key factor in the seismic response of structures. It is important to investigate the time-dependence of this frequency content along the principal directions. For this purpose, moving window Fourier amplitude spectra can be defined at a given frequency ω as (Kubo and Penzien 1976)

$$F_i(\omega, \bar{t}, \Delta t) = \left| \int_{\bar{t}-\frac{\Delta t}{2}}^{\bar{t}+\frac{\Delta t}{2}} a_i(t)\ \mathrm{e}^{-\mathrm{i}\omega t}\ \mathrm{d}t \right| \qquad\qquad i = 1, 2, 3 \tag{8}$$

in which Δt denotes the length of a moving window centered on time $\bar{t}$, and 1, 2 and 3 the time-dependent major, intermediate and minor principal axes, respectively. Such a time-frequency domain analysis allows tracking of the evolution of frequency content along each principal direction as a function of time.

The techniques described above are applied next to determine the principal directions of the ground motions recorded during the Val-des-Bois earthquake and to carry out the corresponding time-frequency analyses. Selected results are illustrated in the next section.

4 Results and discussions

4.1 Covariances and intensity ratios

The covariances μ_{ij} are first evaluated considering : (i) the entire duration of each record, and (ii) a Trifunac-Brady duration (Trifunac and Brady 1975) corresponding to a time interval $\Delta t_{\text{TB}} = t_{\text{f}} - t_0$ during which the earthquake releases between 5% and 95% of its Arias intensity (Arias 1970). Table 2 contains the obtained intensity ratios μ_2/μ_1, μ_3/μ_1, γ_H and γ_V. The results confirm that averaging over a Trifunac-Brady duration yields stable results when compared to averaging over the entire earthquake duration. Using Trifunac-Brady duration also eliminates parasitic effects due to small amplitude fluctuations at the beginning and at the end of the each record. Table 2 also presents mean values and standard deviations of the results considering all the records. Mean ratios $\mu_2/\mu_1 = 0.69$ (respectively $\mu_2/\mu_1 = 0.66$) and $\mu_3/\mu_1 = 0.46$ (resp. $\mu_3/\mu_1 = 0.42$) are obtained considering entire (resp. Trifunac-Brady) durations. These results are lower than the mean ratios $\mu_2/\mu_1 = 0.75$ and $\mu_3/\mu_1 = 0.5$ obtained by Penzien and Watabe (1975) considering the entire durations of records from six ground motions recorded in California and Japan. Mean ratios $\gamma_H = 0.66$ (respectively $\gamma_H = 0.64$) and $\gamma_V = 0.48$ (resp. $\gamma_V = 0.44$) are found considering entire (resp. Trifunac-Brady) durations of all the records. When only ground motions at hard rock sites OTT and OTGH are considered, mean ratios $\gamma_H = 0.64$ (respectively $\gamma_H = 0.61$) and $\gamma_V = 0.43$ (resp. $\gamma_V = 0.40$) are obtained considering entire (resp. Trifunac-Brady) durations of the records. These intensity ratios between the two horizontal and vertical components can be used to feed and calibrate simulated multi-component records in ENA. As explained before, any of the three inequalities presented in Eq. (7) could be expected. However, previous studies of earthquakes from California, Japan and the Pacific Ring of Fire have shown a strong correlation between the vertical principal direction and the minor variance (Penzien and Watabe 1975; Kubo and Penzien 1976; Loh et al. 1982; López et al. 2006). The results of the present work confirm this correlation for the Val-des-Bois records as illustrated by the last column of Table 2 indicating that the vertical principal axis corresponds to the minor component in all the cases except at station OTNM.

4.2 Acceleration time histories and spectral accelerations along principal components

Figure 4 illustrates the time histories of the three acceleration components transformed into principal axes using a Trifunac-Brady duration at each station. By comparing the uncorrelated accelrograms to the recorded data in Figure 2, we can see that the uncorrelation process has a slight effect on the global morphology of the waveforms. The PGA of each set of three uncorrelated acceleration components at all the sites considered is higher, with minimum increase in PGA obtained at site OT006, i.e. $0.0662\,\text{g} \rightarrow 0.0664\,\text{g}$, and maximum increase at site OT004, i.e. $0.0625\,\text{g} \rightarrow 0.083\,\text{g}$. The spectral accelerations S_{A} of the recorded and uncorrelated ground motions are computed and illustrated in Figure 5. These results show that the acceleration spectra of uncorrelated records have basically the same patterns as those of the original ones. A closer look at the curves reveals that the amplitudes of the acceleration spectra of the two horizontal X and Y components become more distinct after uncorrelation, i.e. H_1 and H_2 components. The most apparent cases are those of stations OTGH and

OT004, showing a richer frequency content of the major principal horizontal component H_1 compared to that of principal component H_2. The results also show that the spectral accelerations associated with the vertical component V are shifted towards higher frequencies for some stations such as OTNM or OT006, but this is not the case for all stations.

4.3 Major and minor horizonal principal directions

Major and minor horizonal principal directions obtained using a Trifunac-Brady duration are illustrated in Figure 6. For comparison purposes, the figure also shows the epicentral directions and the fault strike and dip directions from the focal mechanism solutions (Herrmann 2011 ; Global CMT Project 2011 ; Ma and Motazedian 2012). First, these results show that there is no apparent strong correlation between epicentral and horizontal principal directions of the analyzed Val-des-Bois records. We note however that similar principal directions are found at close stations OTT and OTGH located on hard rock of class A, although station OTGH lies on a thin soil layer less than 5 m-thick (Al-Khoubbi and Adams 2004). It is worth to mention that the same horizontal principal directions are obtained using the records at co-located ETNA station OTT and IA station OT012. The horizontal principal components at station OT004, located on rock site of class B, also point to practically the same directions as the previous stations OTT and OTGH. It is seen that the horizontal principal directions on rock sites seem to agree with the southeast-northwest trending of the reverse fault suggested by the focal mechanism solutions, an orientation also consistent with the northeast trending characterizing the faults forming the Ottawa graben, although no causative effects have been established for this earthquake (United States Geologic Survey 2011). The horizontal principal directions at station OTNM, located at the basement of a 4-storey masonry building laying on 40 m-thick soft soil of class E, including a 23 m-thick clay over silty gravel and till, are slightly rotated towards an East-West orientation, which is probably due to local site effects and soil-structure interaction. The importance of local site effects at the other stations can also be estimated from the corresponding horizontal principal directions shown in Figure 6.

4.4 Time-dependency of ground motion principal components

To further investigate time-dependency of the principal components of Val-des-Bois earthquake, a time dependent transformation is carried out next using a moving time window technique as described in Section 3. The principal axes are then determined over successive time intervals with the same length, centered on incremented time values. The length of the moving time window has to be large enough to keep an average representation and reduce local fluctuations. It has also to be small enough to clearly identify important time dependence trends. The results shown hereafter are obtained using a time window length of 4 s, centered on time values $\bar{t}$ incremented by 2 s, to allow a good compromise between appropriate resolution and a satisfactory average representation for each record.

The technique described above is applied to examine the time-dependency of the following six parameters:

– The intensity ratios γ_H and γ_V defined previously;
– The angles θ_H and θ_V defining the orientation of the principal axes at each instant as illustrated in Figure 3.
– A parameter V_{index} introduced to assess time-dependence of the earthquake vertical component and whether it corresponds to the minor, intermediate, or major principal axis, defined as

$$\begin{aligned} V_{\text{index}} &= 1 \qquad \text{if the vertical direction coincides with the minor axis ;} \\ V_{\text{index}} &= 2 \qquad \text{if the vertical direction coincides with the intermediate axis ;} \\ V_{\text{index}} &= 3 \qquad \text{if the vertical direction coincides with the major axis.} \end{aligned}$$

– A intensity parameter $\bar{\sigma}_i$ defined as a normalized running windowed root mean square (RMS) of the principal variance μ_i along each time-dependent principal component $i = 1, 2, 3$

$$\bar{\sigma}_i(\bar{t}, \Delta t) = \left[\frac{\mu_i(\bar{t}, \Delta t)}{\mu_1^{(\max)}} \right]^{\frac{1}{2}} = \left[\frac{1}{\mu_1^{(\max)} \, \Delta t} \int_{\bar{t} - \frac{\Delta t}{2}}^{\bar{t} + \frac{\Delta t}{2}} a_i(t)^2 \, \mathrm{d}t \right]^{\frac{1}{2}} \qquad i = 1, 2, 3 \tag{9}$$

where $\mu_1^{(\max)}$ denotes the maximum of the principal major variance as the center $\bar{t}$ of the moving time window varies along ground motion duration.

Figures 7 and 8 illustrate time variations of six parameters characterizing each station. For comparison purposes, the dashed horizontal lines represent the results obtained using averaging over a Trifunac-Brady duration. The figures show that the intensity functions $\bar{\sigma}_i \,, \; i = 1, 2, 3$ define three stages : a bell-shaped strong motion phase, preceded and followed by two weaker motion segments. Three intensity curves corresponding each to a principal direction could be clearly distinguished. The relative differences in amplitudes between the three curves at each station informs on the relative importance of components in terms of energy content.

The V_{index} bars charts track time-dependent vertical principal direction and its intensity. It is useful to relate the obtained results to the propagation of seismic waves, although the mechanisms involved are generally complex, depending on the type of wave sources and the nature of discontinuities through the crustal structure. It is widely accepted that seismic energy is essentially released through direct primary P-wave propagation at the beginning of a record, and mainly through secondary S-wave and surface wave propagation during the strong motion phase and subsequent portions of the shaking. For all the records at P-wave portion, we find that the vertical direction mainly coincides with the major or intermediate axes, while the two other components are approximately horizontal. Taking into account the longitudinal character of P-waves, this observation suggests their arrival to the recording stations at a relatively deep angle. At the onset of the high intensity S-wave segment and what follows, the vertical principal direction transforms to the intermediate or minor axis as indicated by the V_{index} bars chart in Figures 7 and 8, except at Station OTNM. This behavior suggests that for most of the records, seismic energy is essentially released through the two horizontal principal directions for the entire duration of the shaking.

The γ_H and γ_V ratios can be used to mutually compare the relative importance of the intensities of the principal components as a function of time. First, it can be seen that the ratios γ_H and γ_V vary differently depending on the recording station. The results show that, during the strong motion phase, which is more important to seismic design, the two ratios can be approximated by $\gamma_H^{(\mathrm{TB})}$ and $\gamma_V^{(\mathrm{TB})}$ obtained using a Trifunac-Brady duration. It is also observed that the shape of the γ_V ratio curve approximately follows the V_{index} skyline. This implies that γ_V ratios, and consequently the relative energy released along the vertical direction, are higher when this direction coincides with the major axis, i.e. when $V_{\text{index}} = 3$.

The horizontal and vertical principal angles θ_H and θ_V track the 3D orientation of principal axes during the shaking. Examination of Figures 7 and 8 shows that the horizontal principal angle θ_H exhibits important fluctuations for all the signals processed. No definite trends could be clearly evidenced but it is found that the largest fluctuations correspond to sudden interchanges between the two horizontal principal directions. A similar behavior was observed for other types of ground motions (Penzien and Watabe 1975; Kubo and Penzien 1976; Loh et al. 1982). The figures also reveal that the fluctuations are generally fewer during the strongest motion phase and that θ_H can be correctly approximated by $\theta_{\mathrm{H}}^{(\mathrm{TB})}$ during this portion of the signal. It is noteworthy that the extreme values of $\theta_H = 0\,^\circ$ and $\theta_H = 180\,^\circ$ correspond to instants when the major horizontal principal axis coincides with the epicentral direction. The time-dependence of the vertical principal direction θ_V is generally more stable than θ_H. Although the fluctuations of the horizontal and vertical principal angles are more significant than those obtained for the γ_H and γ_V ratios, they can still be approximated by $\theta_{\mathrm{H}}^{(\mathrm{TB})}$ and $\theta_{\mathrm{H}}^{(\mathrm{TB})}$ over the strong motion phase of the earthquake.

4.5 Time-frequency signatures along principal components

To compare frequency content along each acceleration principal component and to simultaneously track its time evolution, we propose the following normalized spectral amplitude coefficient

$$\alpha_i(\bar{t}, \Delta t) = \frac{G_i(\bar{t}, \Delta t)}{H(\bar{t}, \Delta t)} \qquad\qquad i = 1, 2, 3 \tag{10}$$

where

– the function $G_i(\bar{t}, \Delta t)$ denotes the maximum spectral amplitude obtained over the entire frequency range of interest along principal direction $i = 1, 2, 3$ at time $t = \bar{t}$

$$G_i(\bar{t}, \Delta t) = \max_j \Big[F_i(\omega_j, \bar{t}, \Delta t) \Big] \qquad\qquad i = 1, 2, 3\,; \qquad j = 1 \ldots n_{\mathrm{F}} \tag{11}$$

in which the moving window Fourier amplitude spectra $F_i(\omega_j, \bar{t}, \Delta t)$ are obtained using Eq. (8) at n_{F} discrete frequencies ω_j.

– the function $H(\bar{t}, \Delta t)$ denotes the maximum spectral amplitude value obtained along the three prin-

cipal directions $i=1,2,3$ at time $t=\bar{t}$

$$H(\bar{t},\Delta t)=\max_{i}\Big[G_i(\bar{t},\Delta t)\Big] \qquad\qquad i=1,2,3 \tag{12}$$

To eliminate high frequency oscillations, Fourier amplitude spectra are smoothed by applying Hamming spectral windowing (Båth 1974). Normalizing frequency amplitudes as in Eq. (10) provides a convenient way of evaluating and comparing time-dependent frequency content along each principal direction. Spectral amplitudes are evaluated for discrete frequency values at increments of 0.01 Hz from 0.1 to 10 Hz for all the studied records. This frequency range was selected since it is of most interest in structural response analyses. The time-dependent principal axes are determined considering successive time windows having a length of 4 s, centered on time values $\bar{t}$ incremented by 2 s as previously. Figure 9 illustrates bar charts representing, respectively, the variations of the normalized parameter $\alpha_i(\bar{t},\Delta t)$, for major, intermediate and minor principal components at the different recording stations for different times $\bar{t}$ along a shaking duration of 50 s. As expected, the results show that frequency content varies as a function of each record's location and principal components. We first observe that the time-frequency analyses give practically the same results at stations OTT and OT012, which confirms the good agreement between the accelerograms at the co-located ETNA and IA instruments. The bar charts clearly show that spectral amplitudes along the major principal direction are higher than those along the intermediate and minor components. The spectral amplitudes along the minor principal component are generally of the same magnitude or less than those along the intermediate component. Another finding from Figure 9 is that, for most stations: (i) maximum spectral amplitudes occur practically at the same time, and (ii) the shape of spectral amplitudes over the duration of records are roughly similar along the three principal directions up to a scaling factor variable from station to station. This means that the time-frequency signatures of ground motion components at most stations differ mainly by spectral amplitudes while having practically similar frequency content distributions along the duration of the earthquake. It is important to note that these results are sensitive to the frequency range considered for the analysis, and that they are mainly meant to compare the relative distribution of spectral amplitudes and frequency content between the three principal components over a given frequency range and time interval.

4.6 Relation to ground motion trajectories through a new hodograph representation

To better illustrate local site effects on the three-component records at the different stations, the trajectories of these records are determined based on the displacement time-histories u_X, u_Y and u_Z along the X, Y and Z recording axes, respectively. The displacements used were processed by Atkinson and Assatourians (2010)(Atkinson 2011). A new hodograph representation is proposed herein to highlight the correlation between accelerations and displacements at various time increments along ground motion trajectories at each recording station. For this purpose, the trajectories are constructed as polygons made of successive rectangular segments corresponding each to a time increment from earthquake duration. The face of each segment of the trajectory is obtained by connecting vertices corresponding to the displacements u_X, u_Y and u_Z. The face of each segment of the trajectory is colored to correspond

to the value of the total acceleration $a_{\mathrm{T}} = \sqrt{a_X^2 + a_Y^2 + a_Z^2}$ within the same time increment. This procedure is programmed using MATLAB ® (2011) to obtain the 3D trajectory of a ground motion during any time interval $[t_0,\, t_{\mathrm{f}}]$ of the total duration of the shaking. The 2D XY, XZ and YZ projections of the obtained 3D trajectories are illustrated in Figures 10 to 12, respectively, where a uniform scaling is applied for comparison purposes. For the sake of clear visualization and practical reading of the trajectories, we note that a Trifunac-Brady duration is used instead of the total duration of the shaking, and that the total accelerations a_{T} are normalized by the maximum total acceleration $a_{\mathrm{T}}^{(\mathrm{max})}$ at each site. The presented trajectories have to be analyzed with caution since displacement time-histories are generally very sensitive to numerical integration processing and high instrumental noise levels. Figures 10 to 12 show that the displacement trajectories at stations OTT and OTGH, corresponding to rock sites of classe A, are quite similar and have the smallest amplitudes. The trajectories also suggest that the larger displacements correspond to higher accelerations. We clearly see that the displacement trajectory at IA station OT012 is different from that at the coincident ETNA station OTT. This result, in contrast with the similar principal components obtained from the accelerograms at the two co-located stations, confirms the lower reliability of displacements obtained from IA station OT012 which was reported to have a high instrumental noise level (Adams 2007). The displacement trajectory at station OTNM located on soft soil class E, reveals an important amplification, of approximately 4 times horizontally and twice vertically, relative to the hard rock sites. Again, it can be seen that higher accelerations are recorded mostly at larger displacements at the extremes of the trajectory. Less horizontal and vertical amplifications are observed at station OTRS also located on soft soil class E. The trajectories at the other IA stations seem to indicate more important displacements, especially in the vertical direction, but these results has to be interpreted with caution as mentioned previously. Figure 13 illustrates the XY projections of the displacement trajectories superposed to the horizontal principal components to identify potential correlations. We observe that in most cases, the major principal direction corresponds to segments of the trajectories with moderate to high accelerations, indicating intervals of important energy dissipation during particle motion.

5 Summary and conclusions

The characteristics of three-component ground motions recorded during the $M_{\mathrm{w}}\,5.2$ Val-des-Bois (Québec) earthquake were investigated in this paper. The instrument-corrected records analyzed were provided by a strong motion monitoring network, comprising accelerometers located at sites with different soil conditions, varying from bedrock to thick layers of clay, at epicentral distances ranging from 45 km to 65 km. The correlations between the three ground motion components recorded at different stations were first investigated to understand the individual contributions of each component to the total energy content during the shaking. The acceleration time-histories and spectra of the uncorrelated ground motions were obtained as well as the principal directions and the corresponding principal intensities and intensity ratios. The uncorrelated time-histories and spectra were examined in light of the original data to identify the effect on waveform morphology, PGAs and frequency content. The intensity ratios were determined using total and Trifunac-Brady durations of the shaking, and the results

compared well. The mean intensity ratios between the two horizontal and vertical components were determined and compared to those from other ground motions (Penzien and Watabe 1975). The study also confirmed the strong correlation between the vertical principal directions and the minor intensity ratios as established for other earthquakes (Penzien and Watabe 1975; Kubo and Penzien 1976; Loh et al. 1982; López et al. 2006). No obvious correlation could be identified between epicentral and horizontal principal directions, while an excellent agreement was found between the horizontal principal directions on rock sites and the southeast-northwest trending of the reverse fault suggested by focal mechanism solutions. Effects of local site conditions or soil-structure interaction were highlighted at recording stations located on soil. Time-frequency analyses of the uncorrelated ground motions were also carried out to evaluate and compare time-dependent frequency content along each principal direction. Finally, local site effects were investigated further by constructing three-component trajectories of the records using a new hodograph representation emphasizing the correlation between accelerations and displacements at various time increments of the shaking. The obtained displacement trajectories at stations on soft soils clearly illustrate motion amplifications relative to the hard rock sites along the horizontal and vertical planes. They also help in identifying less reliable displacements due to high instrumental noise levels combined to numerical integration processing. Comparison with the principal components reveals that in most cases, the major principal direction corresponds to segments of the trajectories with moderate to high accelerations, indicating intervals of important energy dissipation during particle motion. This work shed more light on the characteristics of three-component ground motions from an important ENA earthquake (Lamontagne et al. 2008 ; Atkinson and Assatourians 2010 ; Geological Survey of Canada 2011). The results presented could be used to calibrate simulated multi-component ground motions in this region.

Acknowledgements

The authors would like to acknowledge the financial support of the Natural Sciences and Engineering Research Council of Canada (NSERC) and the Canadian Seismic Research Network (CSRN).

References

Adams J, Basham PW, Halchuk S (1995) Northeastern north American earthquake potential – New challenges for seismic hazard mapping. Current Research 1995-D, Geological Survey of Canada, pp 91-99.

Adams J (2007) Soil amplification in Ottawa from urban strong ground motion records. In: Proceedings of the 9th Canadian Conference on Earthquake Engineering, Ottawa, Canada. Paper no. 1162.

Al-Khoubbi I, Adams J (2004) Local site effects in Ottawa, Canada - First results from a strong motion network. In: Proceedings of the 13th World Conference on Earthquake Engineering, Vancouver, Canada. Paper no. 2504.

Arias A (1970) A measure of earthquake intensity. In Seismic Design for Nuclear Power Plants, edited by Hansen RJ, MIT Press, Cambridge, Massachussetts, pp 438-483.

Atkinson GM (2011) Engineering Seismology Toolbox, http://www.seismotoolbox.ca. Accessed 30 July 2011.

Atkinson GM, Assatourians K (2010) Attenuation and source characteristics of the 23 June 2010 M 5.0 Val-des-Bois, Quebec, Earthquake. Seismological Research Letters 81:849-860.

Båth M (1974) Spectral analysis in geophysics, Elsevier, Amsterdam.

Bruneau M, Lamontagne M (1994) Damage from 20th century earthquakes in eastern Canada and seismic vulnerability of unreinforced masonry buildings. Canadian Journal of Civil Engineering 21:643-662.

Cassidy JF, Rosenberger A, Rogers GC (2008) Strong motion seismograph networks, data, and research in Canada. In: Proceedings of the 14th World Conference on Earthquake Engineering, Beijing, China.

Geological Survey of Canada (2011) http://earthquakescanada.nrcan.gc.ca. Accessed 15 January 2011.

Global Centroid-Moment-Tensor (CMT) Project (2011) http://www.globalcmt.org. Accessed 27 October 2011.

Herrmann B (2011) Focal mechanism details. http://www.eas.slu.edu/eqc/. Accessed 22 October 2011.

Hunter JA, Crow H, Brooks GR, Pyne M, Lamontagne M, Pugin A, Pullan SE, Cartwright T, Douma M, Burns RA, Good RL, Motazedian D, Kaheshi-Banab K, Caron R, Kolaj M, Muir D, Jones A, Dixon L, Plastow G, Dion K, Duxbury A, Landriault A, Ter-Emmanuil V, Folahan I (2009) City of Ottawa seismic site classification map from combined geological/geophysical data. Open File 6191, Scale 1:80 000.

Kubo T, Penzien J (1976) Time and frequency domain analysis of three dimensional ground motions San Fernando earthquakes. Report no. EERC 76-6, College of Engineering – University of California, Berkeley, California.

Lamontagne M, Halchuk S, Cassidy JF, Rogers GC (2008) Significant Canadian earthquakes of the period 1600-2006. Seismological Research Letters 79:211-223.

Lin L, Adams J (2010) Strong motion records of the Val-des-Bois, Québec, Earthquake of June 23, 2010. Canadian Hazard Information Service Internal Report 2010-1.1, Geological Survey of Canada.

Loh CH, Penzien J, Tsai YB (1982) Engineering analyses of smart 1 array accelerograms. Earthquake Engineering and Structural Dynamics 10:575-591.

López OA, Hernandez JJ, Bonilla R (2006) Response spectra for multicomponent structural analysis. Earthquake Spectra 22-1:85-113.

Ma S, Motazedian D (2012) Studies on the June 23, 2010 north Ottawa MW 5.2 earthquake and vicinity seismicity. Journal of Seismology 16:513-534.

MATLAB ® (2011). The Mathworks, Inc., Natick, MA, USA.

Mitchell D, Tinawi R, Law T (1990) Damage caused by the November 25, 1988 Saguenay earthquake. Canadian Journal of Civil Engineering 17:338-365.

Penzien J, Watabe M (1975) Characteristics of 3-dimensional earthquake ground motions. Earthquake Engineering and Structral Dynamics 3-4:365-374.

Popov EP (1990) Engineering mechanics of solids, Englewood Cliffs, New Jersey: Prentice Hall.

Rosenberger A, Beverley K, Rogers R (2004) The new strong motion seismic network in southwest British Columbia, Canada. In: Proceedings of the 13th World Conference on Earthquake Engineering, Vancouver, Canada. Paper no. 3373.

Trifunac MD, Brady AG (1975) A study on the duration of strong earthquake ground motion. Bulletin of the Seismological Society of America 65:581-626.

United States Geologic Survey (2011) Poster of the Ontario-Quebec border region, Canada earthquake of 23 June 2010. http://earthquake.usgs.gov/earthquakes/eqarchives/poster/2010/20100623.php. Accessed 12 June 2011.

List of tables

Table 1
Station codes, coordinates, epicentral distances, azimuths, peak ground accelerations along instrument axes X (North-South), Y (East-West), Z (Vertical), and site conditions of the records studied.

Station	Latitude/ Longitude	D_E (km)	θ_A (degree)	Comp.	PGA (10^{-2} g)	Instrument site	Soil condition	Site class
OTT	45.394/ -75.717	58.7	196.8	X	4.26	Seismic vault	Bedrock	A
				Y	3.91			
				Z	3.03			
OTGH	45.401/ -75.697	57.5	195.5	X	4.68	Basement of masonry building	Thin soil	A
				Y	6.32			
				Z	2.99			
OTNM	45.412/ -75.689	56.2	195.2	X	5.17	Basement of masonry building	Soil	E
				Y	11.20			
				Z	8.21			
OTRS	45.460/ -75.496	48.9	179.7	X	7.67	Basement of wood building	Soil	E
				Y	7.84			
				Z	8.71			
OT002	45.474/ -75.502	47.3	180.2	X	5.05	Basement of wood house	Clay	D
				Y	5.84			
				Z	5.24			
OT004	45.364/ -75.775	63.3	199.8	X	4.74	Basement of wood house	Clay or till	B
				Y	5.91			
				Z	6.25			
OT006	45.429/ -75.650	53.6	192.6	X	4.42	Basement of wood house	Till	B
				Y	6.62			
				Z	2.97			
OT008	45.350/ -75.642	62.2	190.3	X	5.98	Basement of wood house	Sand	C
				Y	6.08			
				Z	4.03			
OT012	45.394/ -75.717	58.7	196.8	X	3.33	Seismic vault	Bedrock	A
				Y	3.15			
				Z	2.62			

Table 2
Intensity ratios and principal vertical direction of the studied Val-des-Bois recorded ground motions.

Station	Time interval (s)	Intensity ratios μ_2/μ_1	μ_3/μ_1	γ_H	γ_V	Vertical direction V
OTT	[0.00 – 81.92] [a]	0.66	0.38	0.66	0.38	Minor
	[15.79 – 36.47] [b]	0.63	0.35	0.63	0.35	Minor
OTGH	[0.00 – 81.92] [a]	0.62	0.48	0.62	0.48	Minor
	[25.09 – 51.09] [b]	0.58	0.44	0.58	0.44	Minor
OTNM	[0.00 – 163.84] [a]	0.49	0.27	0.27	0.49	Intermediate
	[17.38 – 34.90] [b]	0.43	0.24	0.24	0.43	Intermediate
OTRS	[0.00 – 163.84] [a]	0.88	0.59	0.88	0.59	Minor
	[16.44 – 43.45] [b]	0.90	0.56	0.90	0.56	Minor
OT002	[0.00 – 81.91] [a]	0.85	0.68	0.85	0.68	Minor
	[17.08 – 38.94] [b]	0.84	0.65	0.84	0.65	Minor
OT004	[0.00 – 81.91] [a]	0.49	0.29	0.49	0.29	Minor
	[21.60 – 39.37] [b]	0.46	0.26	0.46	0.26	Minor
OT006	[0.00 – 81.91] [a]	0.78	0.39	0.78	0.39	Minor
	[17.37 – 39.89] [b]	0.74	0.34	0.74	0.34	Minor
OT008	[0.00 – 81.91] [a]	0.70	0.64	0.70	0.64	Minor
	[18.65 – 40.64] [b]	0.67	0.59	0.67	0.59	Minor
OT012	[0.00 – 81.91] [a]	0.72	0.39	0.72	0.39	Minor
	[19.09 – 41.54] [b]	0.69	0.36	0.69	0.36	Minor
	Mean	0.69 [a]	0.46 [a]	0.66 [a]	0.48 [a]	
		0.66 [b]	0.42 [b]	0.64 [b]	0.44 [b]	
	Standard deviation	0.14 [a]	0.15 [a]	0.19 [a]	0.13 [a]	
		0.16 [b]	0.15 [b]	0.20 [b]	0.13 [b]	

[a] Total duration of seismic record.

[b] Trifunac-Brady duration of seismic record.

List of figures

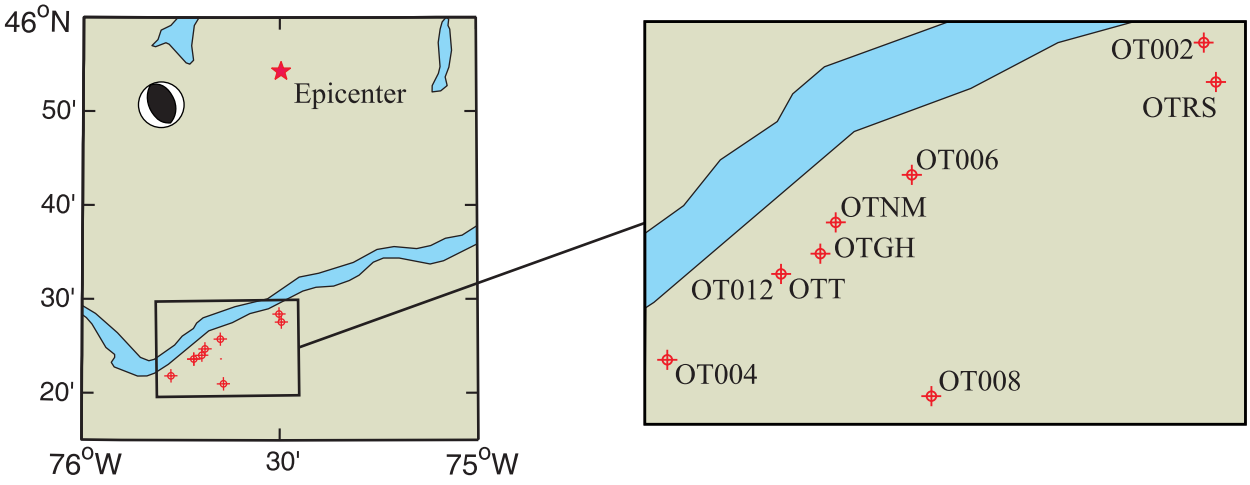

Figure 1. Epicenter of the 23 June 2010 Val-des-Bois earthquake, focal mechanism and recording stations of the ground motions studied.

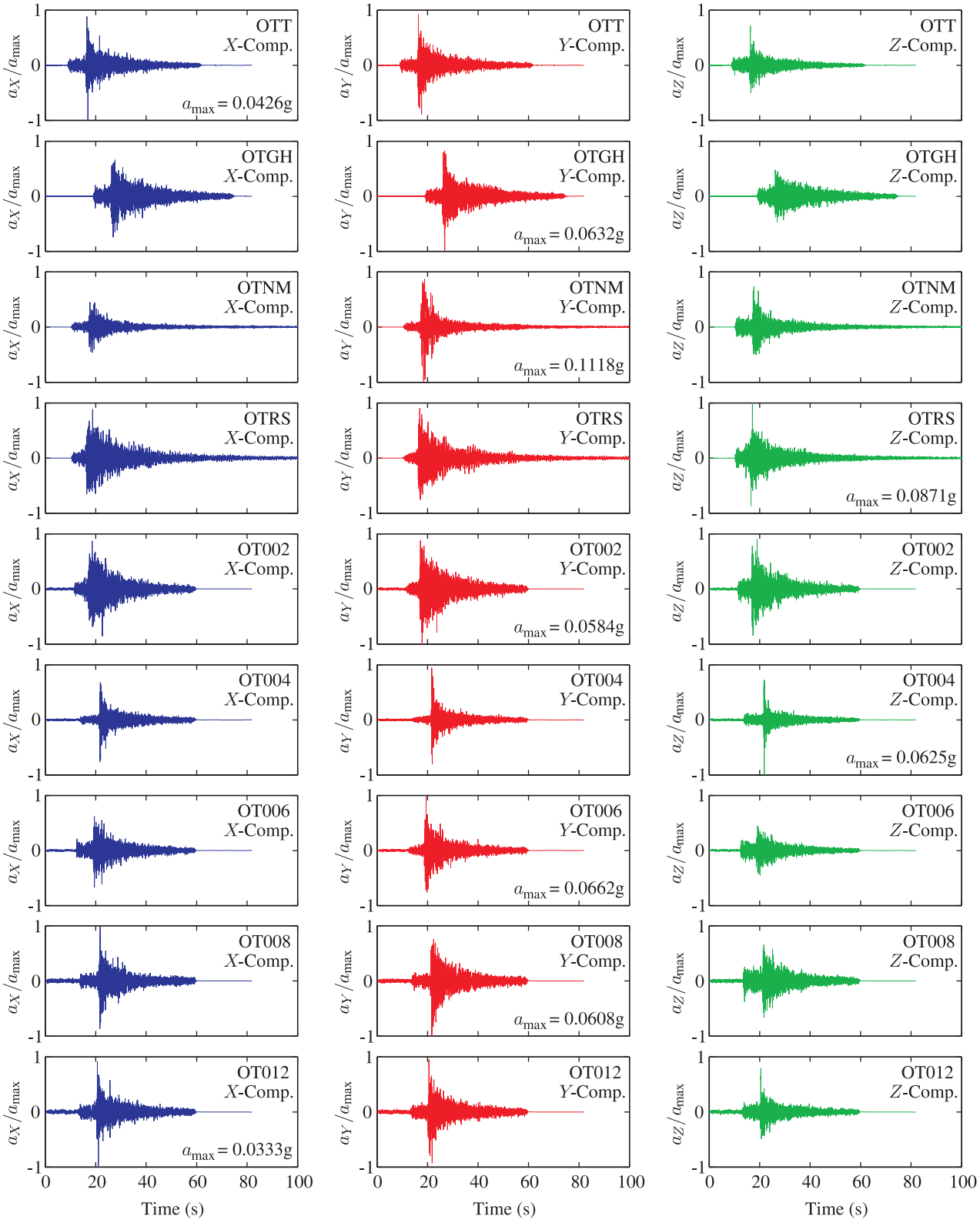

Figure 2. Time-histories of studied accelerations recorded during Val-des-Bois earthquake along instrument axes X (North-South), Y (East-West) and Z (Vertical).

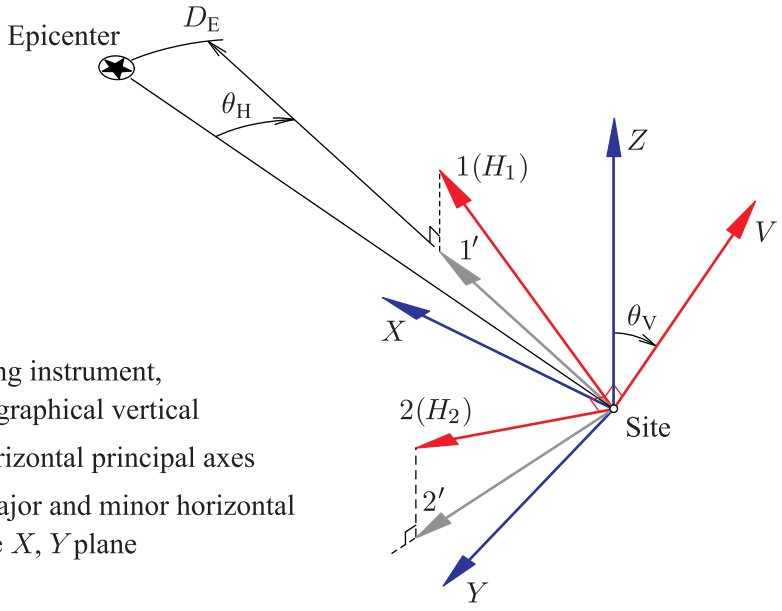

X, Y and Z : Axes of recording instrument,
Z being the geographical vertical

1 and 2 : Major and minor horizontal principal axes

$1'$and $2'$: Projections of the major and minor horizontal principal axes on the X, Y plane

V: Vertical principal axis

Figure 3. Definitions of principal axes and angles.

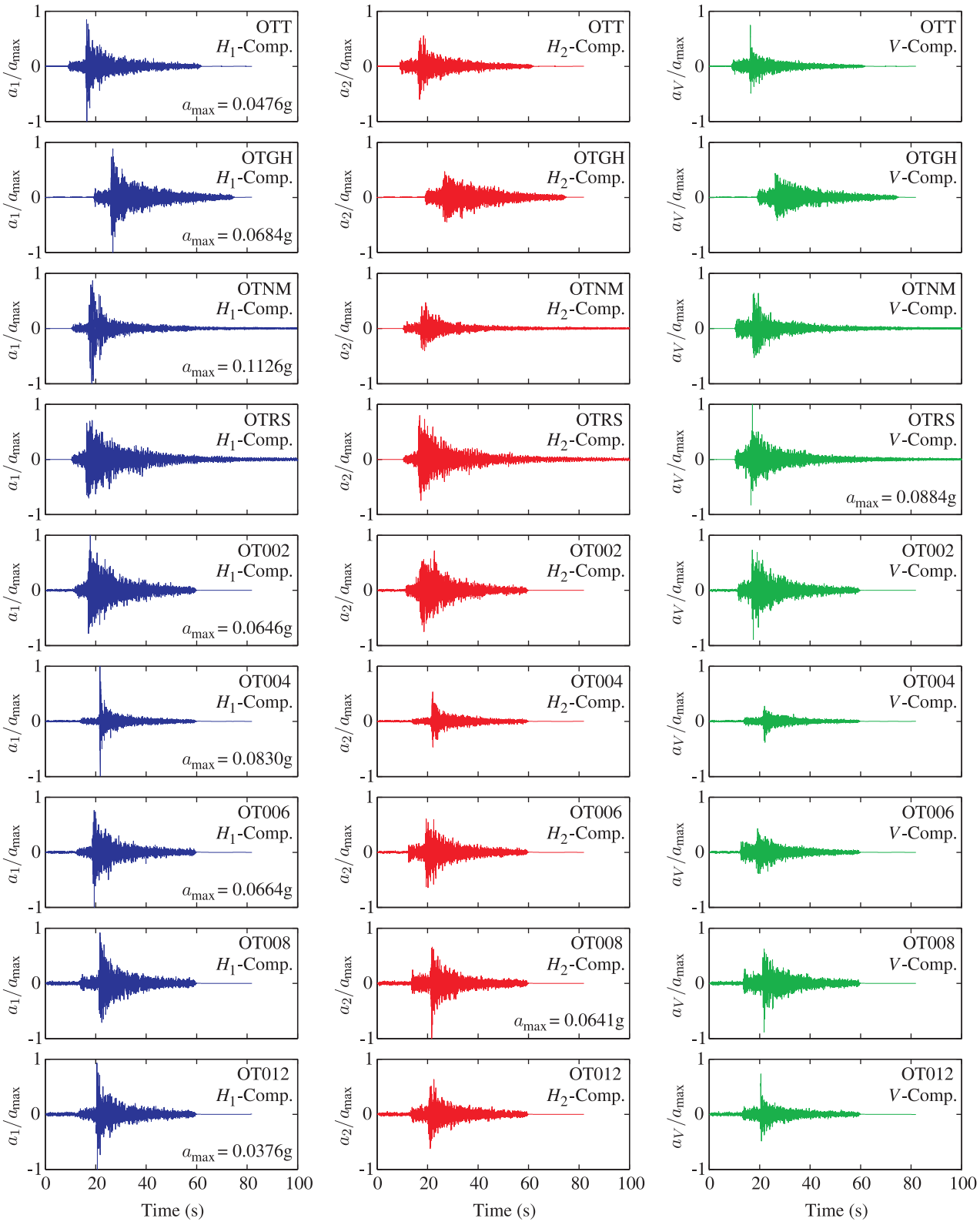

Figure 4. Time-histories of uncorrelated acceleration components H_1, H_2 and V of the studied ground motions of Val-des-Bois earthquake.

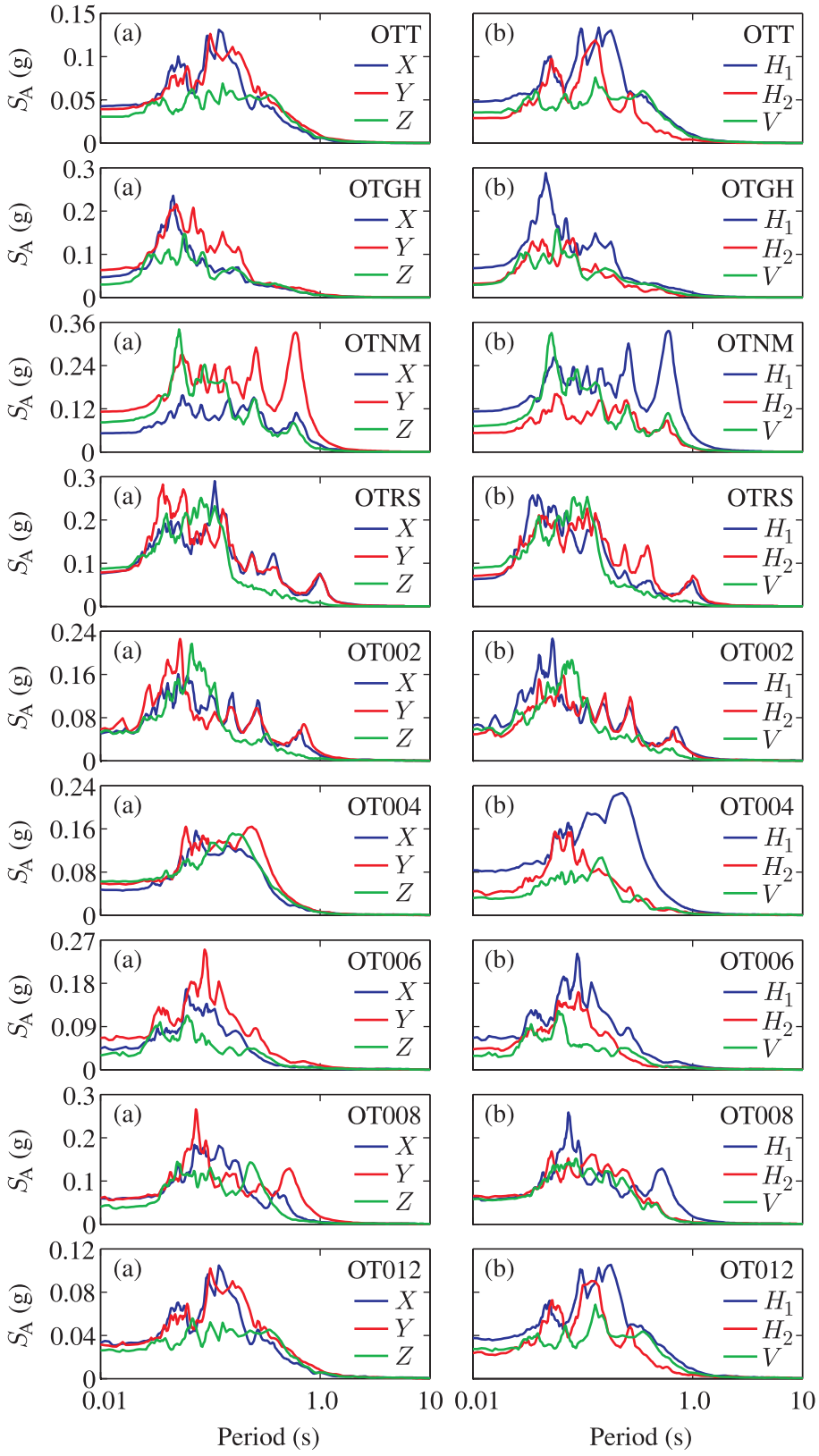

Figure 5. Acceleration spectra of the studied ground motions of Val-des-Bois earthquake: (a) Recorded ground motions; (b) Uncorrelated ground motions.

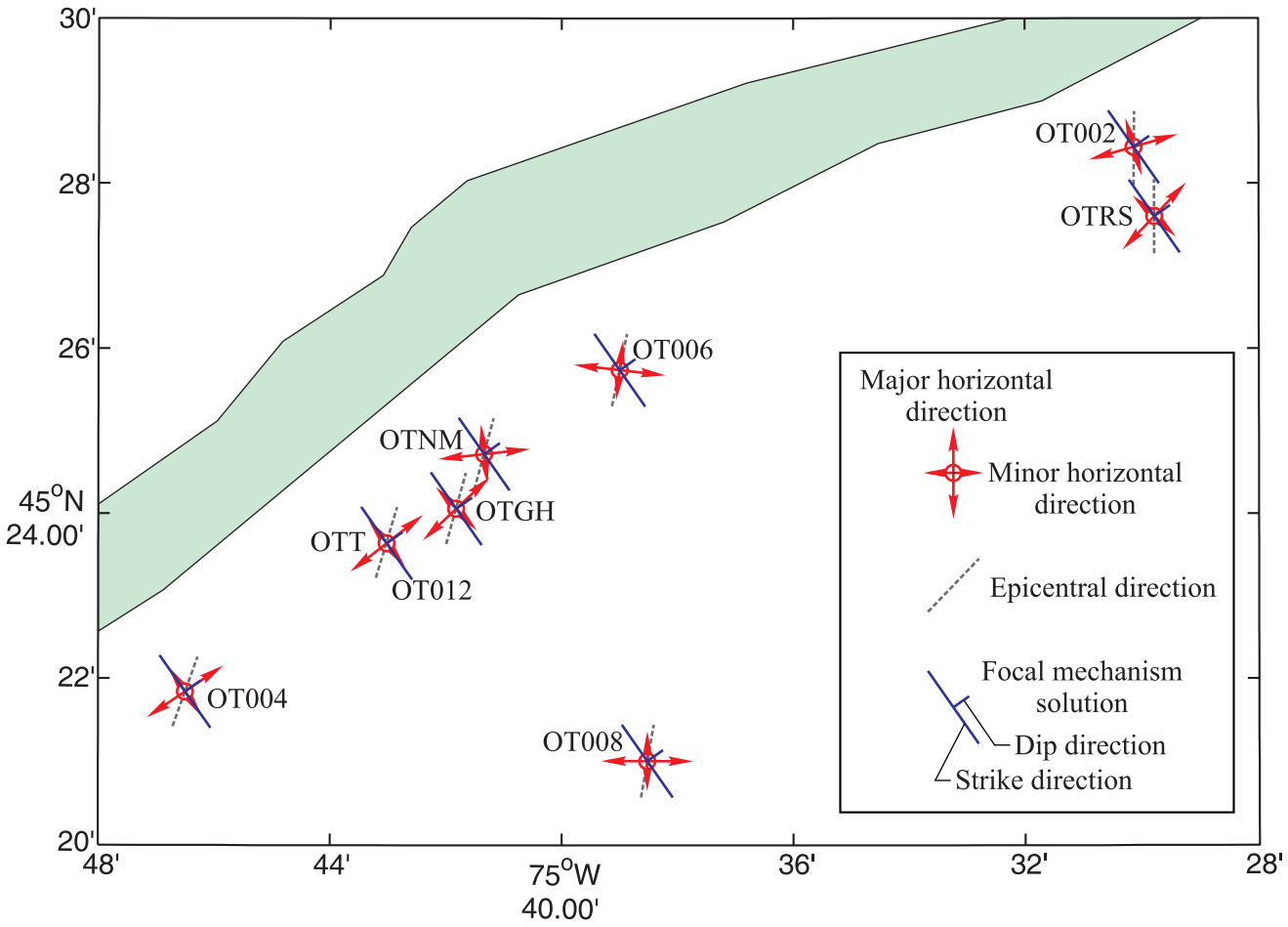

Figure 6. Horizontal principal directions of the studied ground motions of Val-des-Bois earthquake presented at the different stations and superposed to the epicentral directions and focal mechanism solution of the event.

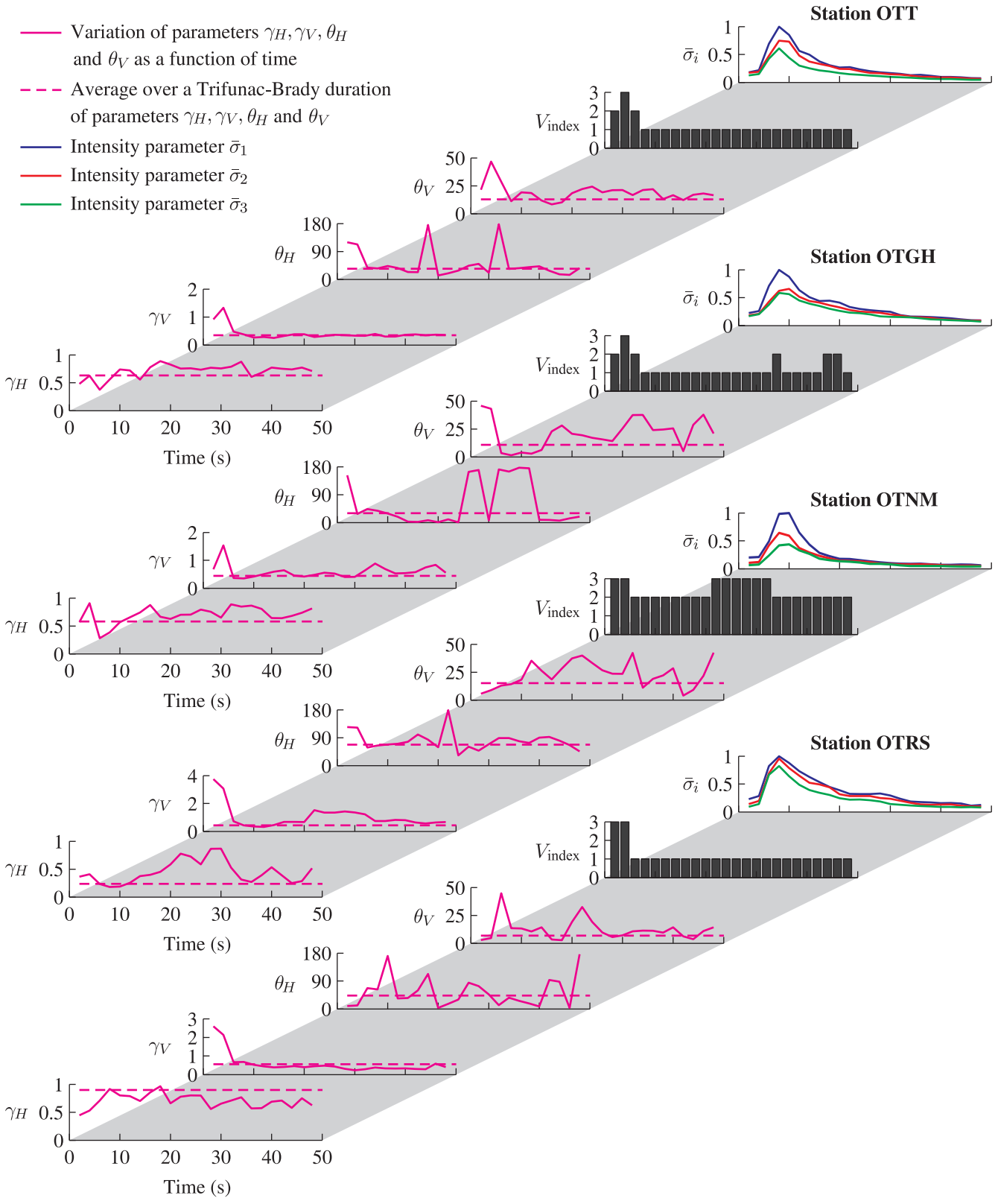

Figure 7. Variation of parameters $\gamma_H, \gamma_V, \theta_H, \theta_V, V_{\text{index}}$ and $\bar{\sigma}_i$, $i = 1, 2, 3$, as a function of time during shaking at stations OTT, OTGH, OTNM and OTRS.

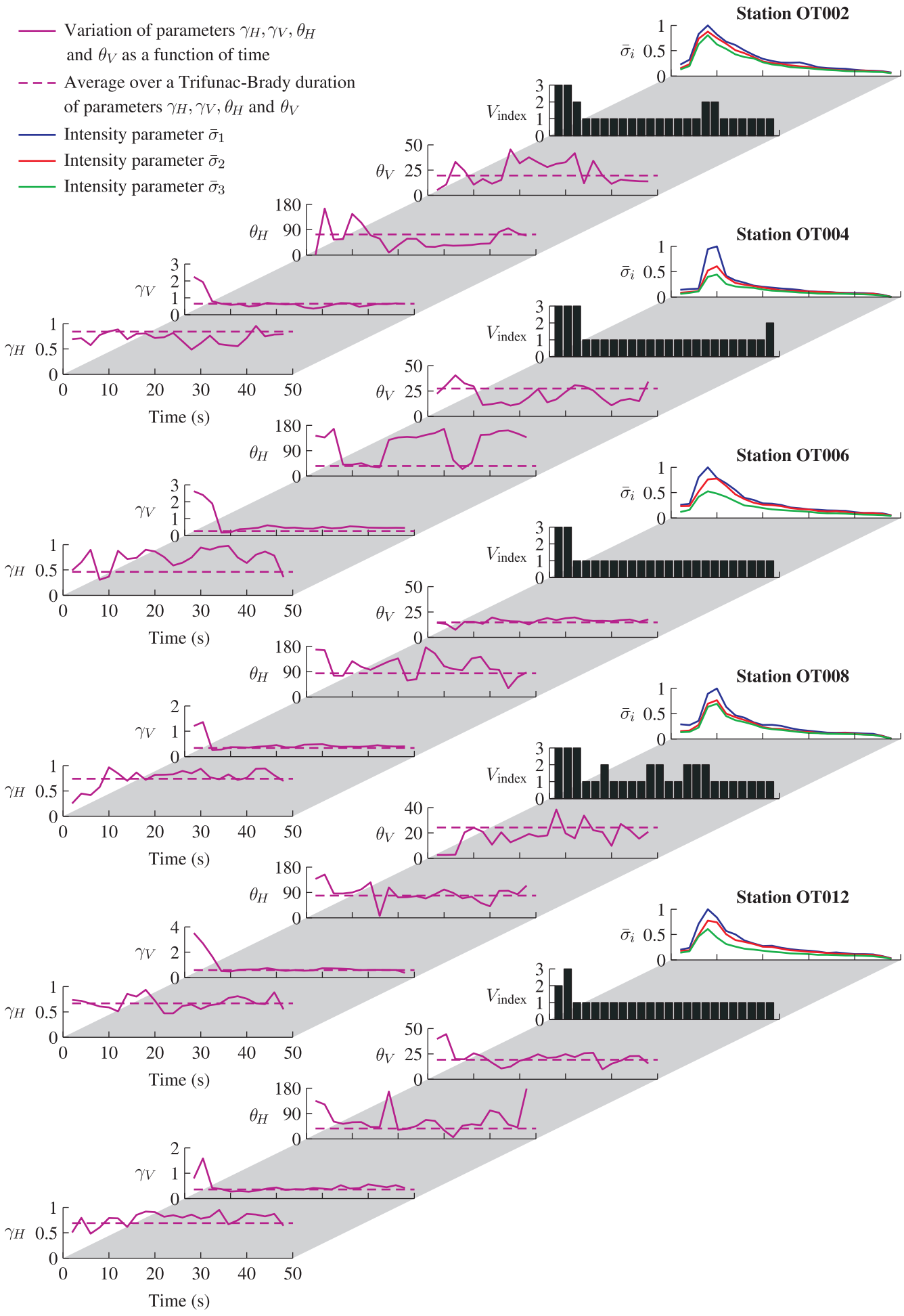

Figure 8. Variation of parameters $\gamma_H, \gamma_V, \theta_H, \theta_V, V_{\text{index}}$ and $\bar{\sigma}_i$, $i = 1, 2, 3$, as a function of time during shaking at stations OT002, OT004, OT006, OT008 and OT012.

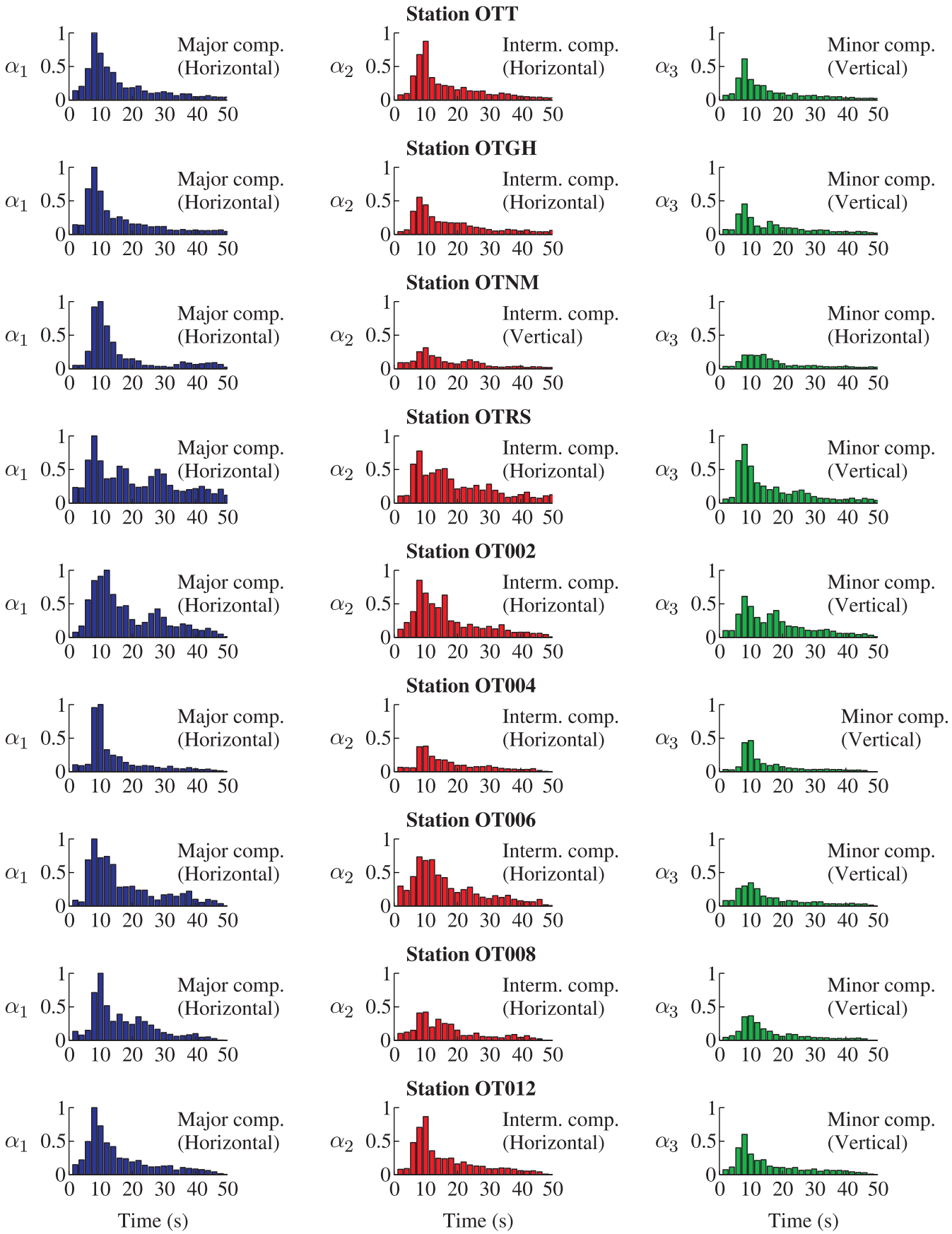

Figure 9. Time-frequency analyses of the uncorrelated three-component ground motions of Val-des-Bois earthquake.

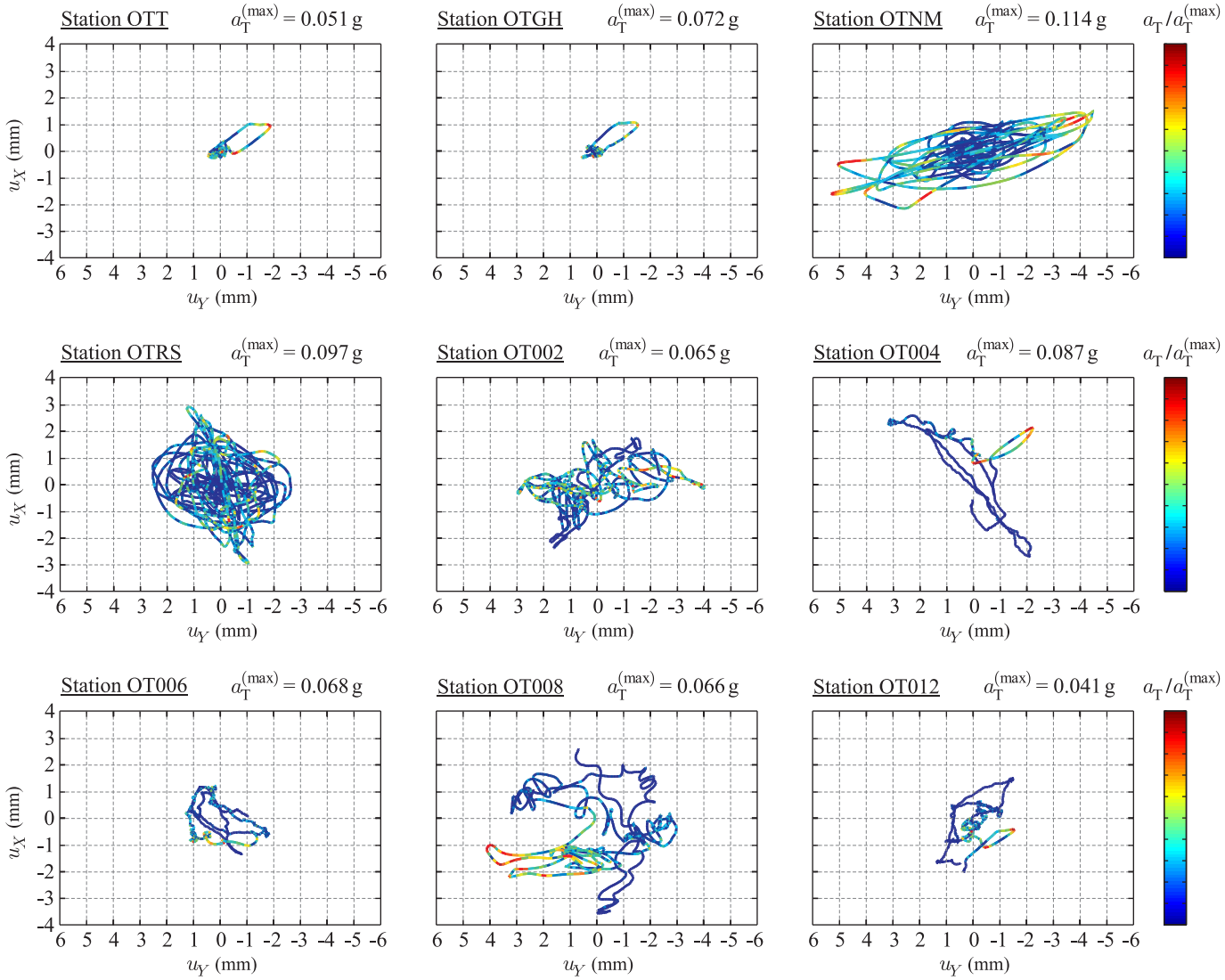

Figure 10. *XY*-projections of the displacement trajectories of the studied recorded ground motions of Val-des-Bois earthquake.

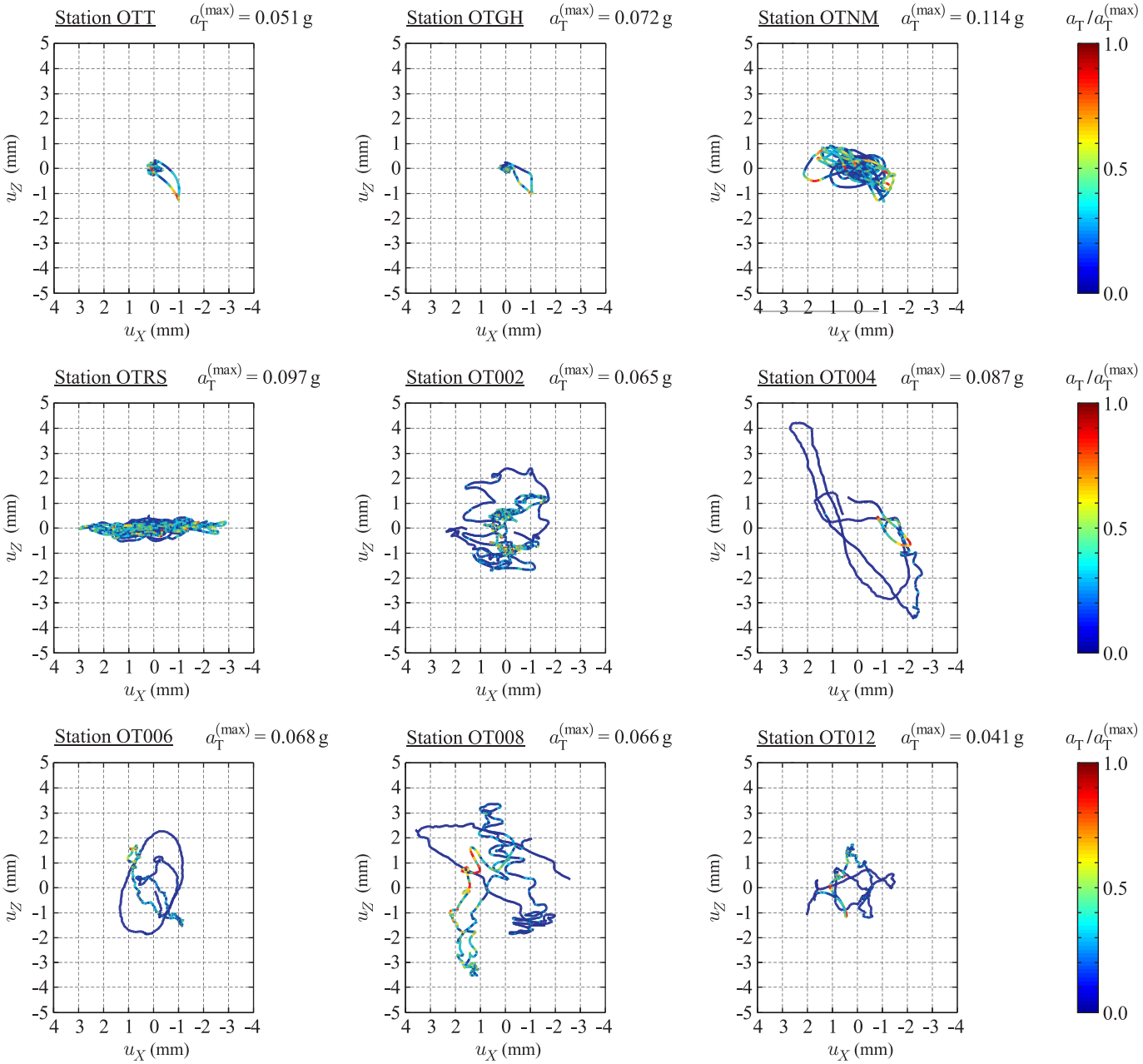

Figure 11. XZ-projections of the displacement trajectories of the studied recorded ground motions of Val-des-Bois earthquake.

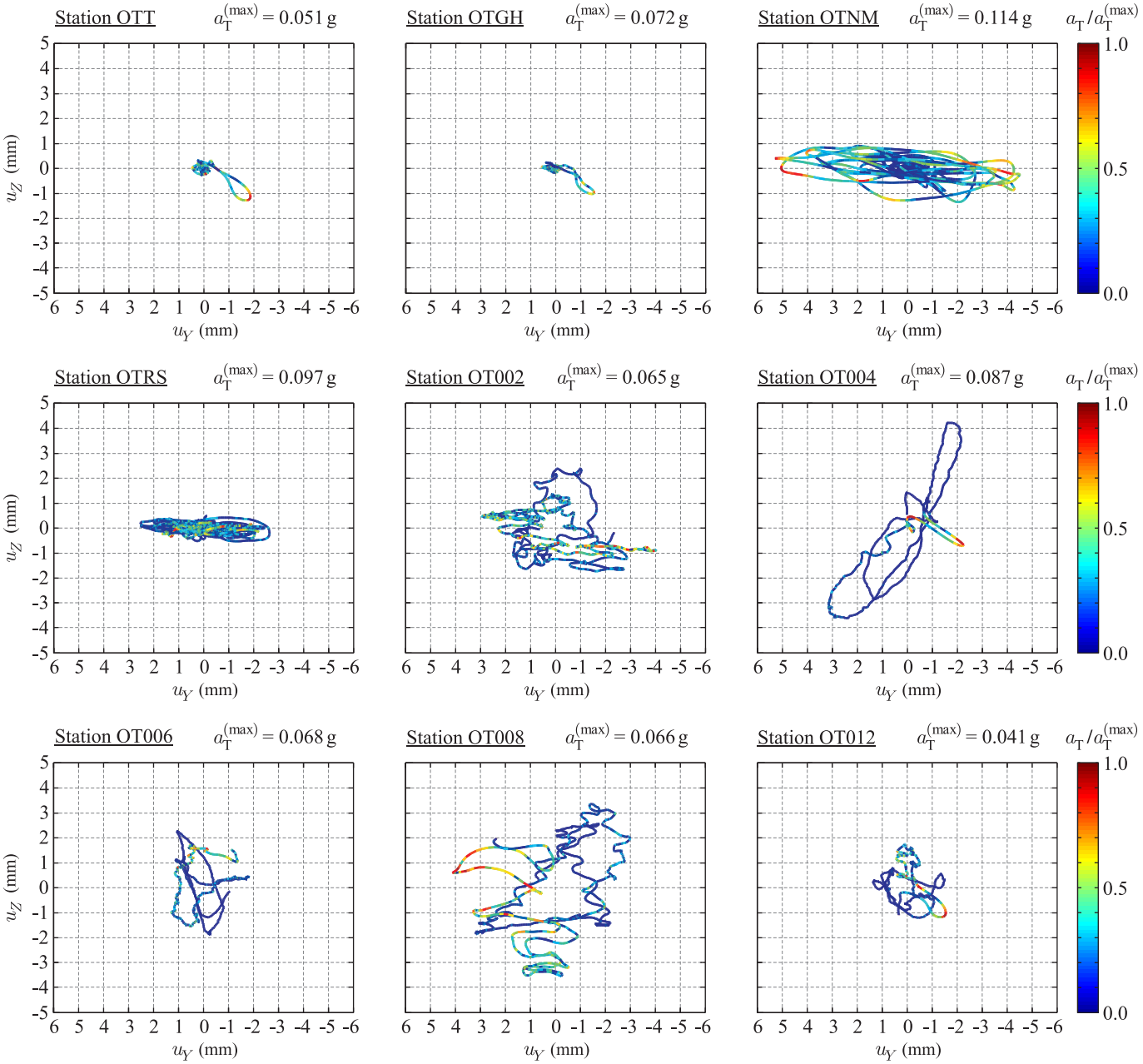

Figure 12. YZ-projections of the displacement trajectories of the studied recorded ground motions of Val-des-Bois earthquake.

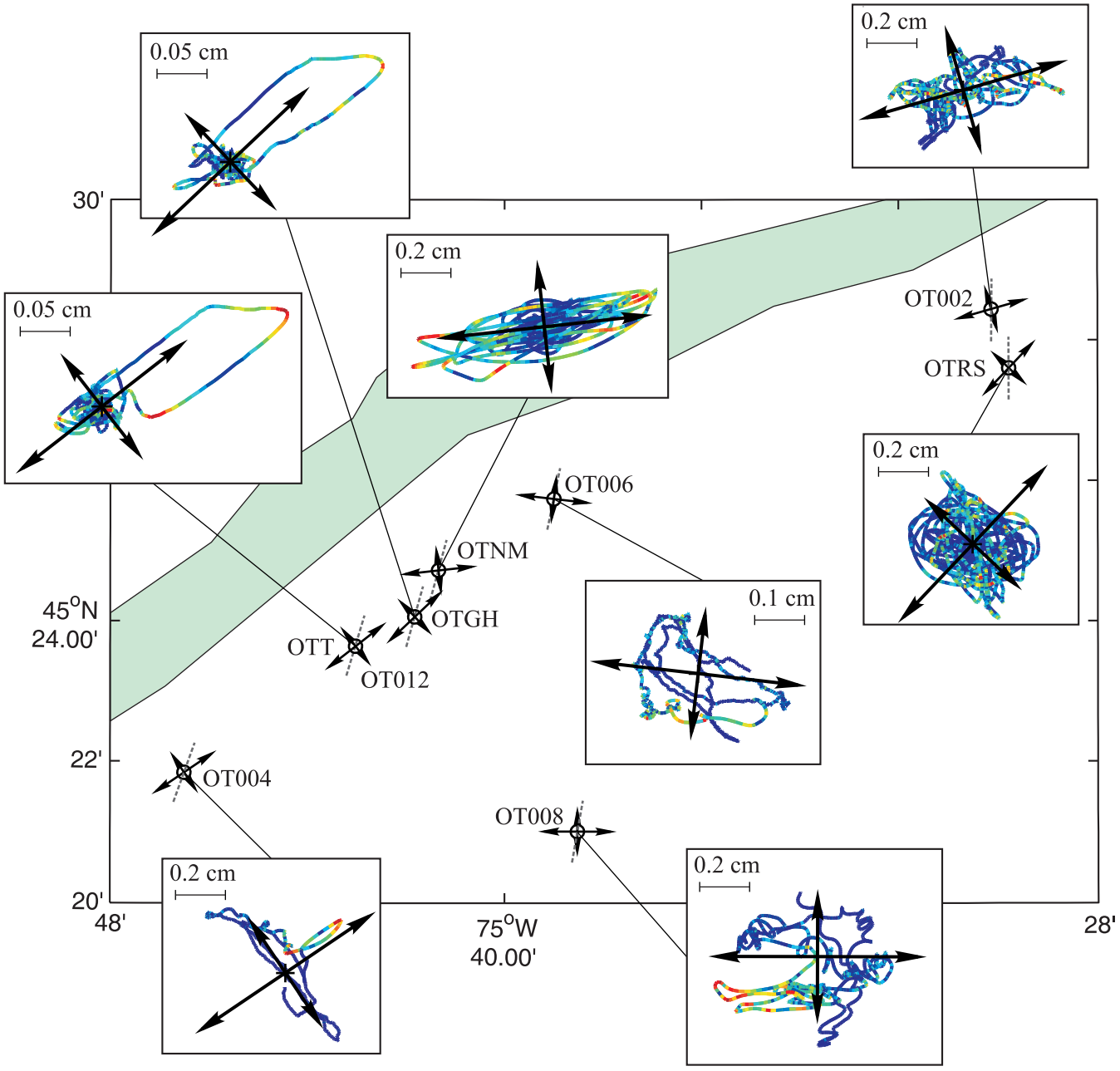

Figure 13. *XY*-projections of displacement trajectories and superposed principal directions of the ground motions of Val-des-Bois earthquake.